Evaporation of water droplets in the 1st stage of the ultrasonic spray pyrolysis device

Izhlapevanje vodnih kapljic v prvi stopnji naprave za ultrazvočno razpršilno pirolizo

Primož Ternik[1], Rebeka Rudolf[2]*

1 Ternik Primož - Zasebni raziskovalec, Bresterniška ulica 163, Bresternica

[2] Faculty of Mechanical Engineering, University of Maribor, Smetanova 17, 2000 Maribor

*Avtor za korespondenco: rebeka.rudolf@um.si

Abstract: The present work deals with numerical modelling of aerosol evaporation in the flow of carrier gas (N_2) in the 1st stage of ultrasonic spray pyrolysis device. For that we have used so called Euler-Lagrange approach, where the gas phase is treated as a continuous phase by solving the Navier-Stokes equations, while the dispersed phase is treated as a number of discrete particles, which exchange energy, momentum and mass with the continuous phase. Results are presented for the temperature field of carrier gas and water vapor, as well as for the droplets' diameter, temperature and evaporation time.

Key words: Evaporation, Numerical modelling, Euler-Lagrange approach, Water droplets.

Povzetek: Numerično smo modelirali proces izhlapevanja aerosola (generiranega iz vode) v toku nosilnega plina (N_2) v prvi stopnji naprave za ultrazvočno razpršilno pirolizo. Uporabili smo t.i. Euler-Lagrangeov pristop, ki obravnava plinsko fazo kot zvezno telo z reševanjem (v primeru turbulentnega toka časovno povprečenih) Navier-Stokesovih enačb, razpršeno fazo pa kot veliko število diskretnih delcev (mehurčkov, kapljic ali trdnih delcev), ki si z zvezno fazo izmenjujejo energijo, gibalno količino in/ali maso. Prikazani so rezultati za temperaturno polje nosilnega plina in aerosola, kakor tudi za premer, temperaturo ter čas izhlapevanja vodnih kapljic. Le ti kažejo, da je izhlapevanje najintenzivnejše v začetnem delu grelnega območja in da relativna vlažnost nosilnega plina nima pomembnega vpliva na sam proces izhlapevanja.

Ključne besede: izhlapevanje, numerično modeliranje, Euler-Lagrange pristop, vodne kapljice.

1. Introduction

The term nanomaterial determines the whole group of materials that are consisting of structure components that have at least one dimension in nanometre scale [1]. Some macroscopic objects, thin films and powders also belong to this group as long as they are made of nanoparticles, nanocrystals, nanopores or other forms in nanoscale. One example for classification of nanostructures is given in Fig. 1.
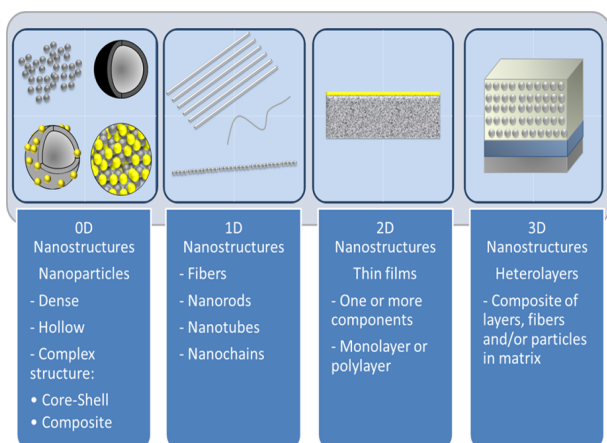

Figure 1. Classification of nanostructures in terms of their dimensions [1].

As the nanotechnology was developing, it came to need to classify existing nanostructured materials. One of the first classifications was done by Gleiter (1995) and it was further developed with the development of nanotechnology itself. The classification in the Fig. 1 is mostly based on the proposed classification of Pokropivny and Skorokhod (2006) [1], which is constituted on dimensionality of nanostructured materials. As it can be seen, there are four groups of materials, zero-, one-, two- and tree- dimensional materials and each of them has various subgroups. In the scope of this research, only zero-dimensional nanostructures are going to be studied. In this group of nanostructures belong nanoparticles and clusters of nano-particles. Based on IUPAC definition, the nanoparticles are particles of any shape with dimensions in the range 1×10^{-9} and 1×10^{-7} [2]. This limit of 100nm is taken due to fact that particles smaller than 100nm have some novel properties, different than the bulk material. In some cases is this upper limit extended to 500nm, but this limit is also matter of debate, since some particles with diameter bigger then 500nm still may be consisted of nanocrystals smaller than 100nm.

Up to now, many nanoparticles have been synthesized by various techniques including sol-gel method, chemical vapour deposition, precipitation method, laser vaporization condensation method, and ultrasonic spray pyrolysis (USP) method. Among these techniques, USP process has been successfully applied for the synthesis of spherical nanoparticles with controlled and uniform particle size. Unlike physical vapour deposition methods, USP does not require high quality target and nor does it require vacuum at any stage, which is of great advantage if this technique is to be scaled-up for the industrial applications. Furthermore, the USP has many other advantages, like high purity of synthesized particles, regular shape of particles, and better control of chemical stoichiometry.

The particles generated in USP are based on a one-droplet-to-one-particle conversion mechanism [3]. The atomized precursor to droplet formation is introduced into a heated region by a carrier gas under atmospheric pressure conditions. Inside the furnace, the solvent in the droplets evaporates, and the remaining solutes evolve precipitation, thermal decomposition and interparticle reactions to form product particles. A droplet can be assumed to be a "microreactor", producing a spherical submicron-sized particle.

In general, the particle size is determined by the initial droplet size and precursor concentration. However, the investigation of Ogi et al. [4] showed that not only controlled pressure but also other operating conditions, such as temperature, carrier gas flow rate and the proper selection of the precursor and its composition as a starting material, are the key factors to obtain nanoparticles.

While the on-site experimental testing provides the most direct assessment of precursor droplets evaporation process, often the cost and availability of testing is limited or even impossible. Therefore, the computational fluid dynamics (CFD) for this type of application has become very useful. The objective of the present study is to numerically investigate the evaporation process of water droplets in the pilot USP device. For this we will use the Euler-Lagrange approach, where the conservation equations of the continuous gaseous phase were solved and coupled with the discrete droplets phase.

2. Numerical model

The simulation performed involves the evaporation of water droplets in the carrier gas (nitrogen) flow. The numerical modelling of the phenomenon was carried out by adopting an Eulerian-Lagrangian approach. In this approach a Lagrangian phase (water droplets) move within a continuous Eulerian phase (nitrogen). Water droplets are spherical, therefore the simulation do not

consider the degree of deformation caused by nitrogen friction.

2.1 Continuous phase

The continuous phase was modelled as laminar flow an ideal gas mixture of nitrogen (carrier gas) and evaporated water vapour. For both mixture species the temperature dependent physical properties were accounted for [5].

2.2 Discrete phase

The trajectory of a discrete phase is determined by integrating the force balance on the droplet, which is written in a Lagrangian reference frame. This force balance equates the droplet inertia with the drag force acting on the droplet, and can be written as:

$$\frac{d\vec{v}_p}{dt} = F_D\left(\vec{v} - \vec{v}_p\right) + \frac{\vec{g}(\rho_p - \rho)}{\rho_p} + \vec{F} \tag{1}$$

where $\vec{F}$ is an additional acceleration term, $F_D\left(\vec{v} - \vec{v}_p\right)$ is the drag force per unit droplet mass

$$F_D = \frac{18\eta}{\rho_p d_p^2}\frac{C_D Re}{24} \tag{2}$$

Here, $\vec{v}$ is the fluid phase velocity, $\vec{v}_p$ is the discrete phase velocity, η is the dynamic viscosity of the fluid, ρ is the fluid density, ρ_p is the density of the discrete phase, and d_p is the droplet diameter. Re is the relative Reynolds number

$$Re = \frac{\rho d_p|\vec{v}_p - \vec{v}|}{\eta} \tag{3}$$

and $C_D = a_1 + a_2/Re + a_3/Re^2$ is the drag coefficient for smooth particles [6].

The heat and mass transfer between gas phase and droplet takes place at the interface of the droplet and the surrounding gas. Whenever a water droplet is in contact with a gas stream, a film of saturated gas-vapour is formed on the droplet surface. Heat transfer takes place if a temperature difference exists between the liquid temperature at the surface and the gas dry-bulb temperature. Additionally, mass transfer takes place if a vapour concentration gradient exists between the vapour layer and the ambient gas.

The heat balance relating the sensible heat change in the droplet to the convective heat transfer between the droplet and the gas phase is

$$m_p c_p \frac{dT_p}{dt} = hA_p\left(T_\infty - T_p\right) - \frac{dm_p}{dt}h_{fg} \tag{4}$$

where m_p is the mass of the droplet, c_p is heat capacity of the droplet, T_p is the droplet temperature, A_p is the surface area of the droplet, T_∞ is the local temperature of the gas phase, h_{fg} is the latent heat, and h is the convection heat transfer coefficient, which is obtained by the empirical correlation of Ranz and Marshall [7]

$$Nu = 2.0 + 0.6Re^{1/2}Pr^{1/3} \tag{5}$$

where the Prandtl number Pr refers to the continuous phase.

Mass transfer (mass loss) of the droplet due to evaporation is calculated as [8, 9]

$$\frac{dm_p}{dt} = ShA_p\rho_\infty \ln(1 + B_m) \tag{6}$$

where Sh is the Sherwood number, A_p surface area of the droplet, ρ_∞ is density of bulk phase. B_m is the Spalding mass number given by

$$B_m = \frac{Y_{i,s} - Y_{i,\infty}}{1 - Y_{i,s}} \tag{7}$$

where $Y_{i,s}$ and $Y_{i,\infty}$ are the vapour mass fractions at the surface and in the bulk phase.

2.3 Geometry and boundary conditions

The problem of the water droplets evaporation in carrier gas flow is depicted schematically in Fig. 2. The tubular furnace was a quartz tube with an inside diameter of $0,021m$ and length of $0,80m$. Nitrogen, as the carrier gas, was kept at flow rate of $1.5l/min$.
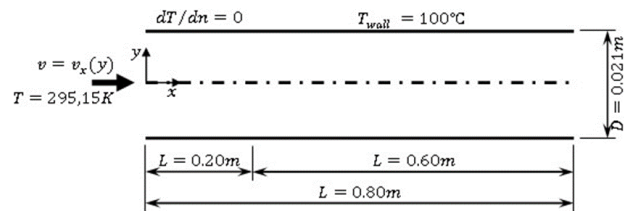

Fig. 2. Geometry and boundary conditions.

The inlet, wall and outlet were employed as boundary conditions. The wall boundary conditions represented the surface of the tube wall; for the unheated part we have prescribed adiabatic wall

boundary conditions (i.e. zero heat flux), while the heated tubular furnace was kept at constant heating temperature of $100°C$.

Finally, the water droplets (with volume flow rate $20\,ml/h$) of initial diameter $5\mu m$ and temperature $295.15K$ were injected at $x = 0.18m$.

In the present numerical study we have considered the following cases:

- Case 1: Carrier gas flow without water droplets
- Case 2: Carrier gas flow + water droplets; relative humidity of carrier gas flow $\varphi = 0\%$
- Case 3: Carrier gas flow + water droplets; relative humidity of carrier gas flow $\varphi = 20\%$

3. Results

3.1 Model verification

There is a lack of validation cases for evaporation of droplets having diameters less then $50\mu m$. For that, the present study has been by validated by studying the evaporation of single water droplet (initial diameter: $200\mu m$, initial temperature: 50˚C) suspended in still humid air (relative humidity: 20%, temperature: 50˚C). Comparison of present results with the results of Alroe [10] shows that present CFD model correctly captured the evaporation of the single droplet, thereby verifying our modelling approach (Fig. 3).
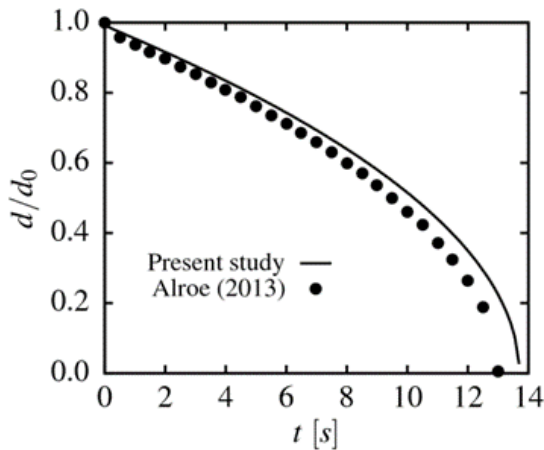
Fig. 3. Comparison of the droplet diameter reduction between the present results and the results of Alroe [10].
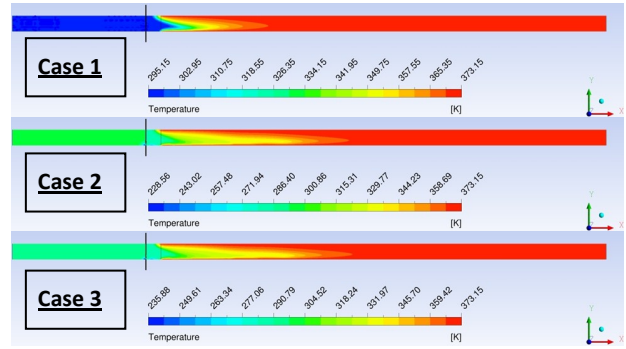
3.2 Evaporation of water droplets

Fig. 4. Temperature distributions on a vertical mid-plane $(z = 0.0)$.

Fig. 4 shows temperature distributions on a vertical mid-plane of the heated tube. The temperature of the upper wall region of the tube is higher than that of the bottom wall region. As the carrier gas passes through the heated zone and its temperature is increased, its velocity vector gains an upward component due to the effect of buoyancy. Accordingly, hotter carrier gas exhibits motion in the upward direction associated with its motion in the axial direction (Fig. 5).
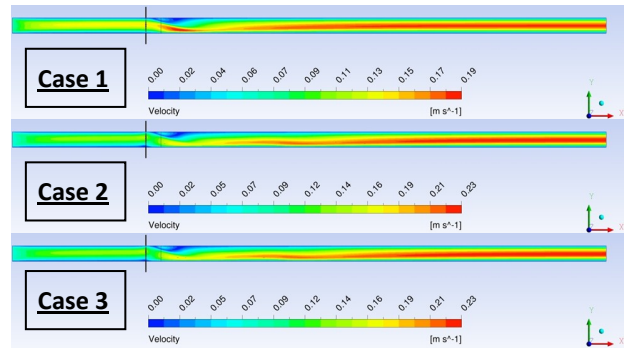
Fig. 5. Axial velocity distributions on a vertical mid-plane $(z = 0.0)$.

With respect to the temperature distributions obtained (Fig. 4), the lowest temperature gradient is produced in the lower wall region, and consequently, the slower evaporation rate of the liquid phase can be expected. On the other hand, higher temperature regimes (in the upper wall region) could cause faster heating and cooling, with steeper temperature gradients associated with the introduction of higher energy for water droplets evaporation (Fig. 6). One can also conclude that the relative humidity of a carrier gas has no significant affect on the evaporation process (Tab. 1).
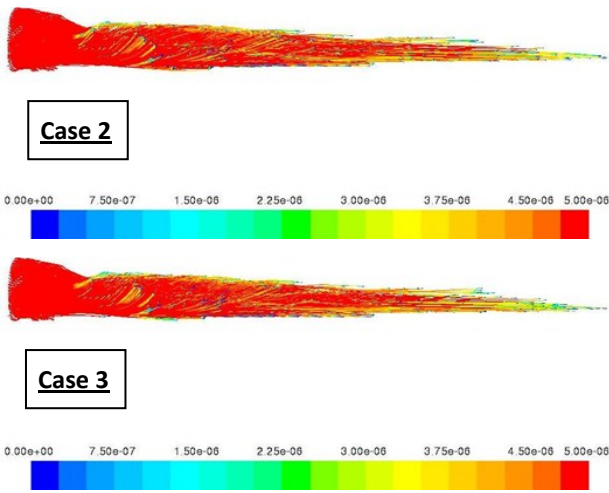
Fig. 6. Diameter variation of evaporating water droplets.

Table 1. Influence of relative humidity on the evaporation process of water droplets.

	Relative humidity of	Evaporation time	Evaporation length
Case 2	0%	1.75s	0.192m
Case 3	25%	1.81s	0.194m

4. Conclusions

The present work deals with numerical modelling of water droplets evaporation in the flow of carrier gas (N$_2$) in the 1st stage of ultrasonic spray pyrolysis device. For that we have employed Euler-Lagrange approach, where the gas phase is treated as continuum, while the water droplets are treated as discrete particles.

The numerical model was validated for the case of single droplet evaporation in a surrounding stationary humid air for which the results are available in an open literature. Remarkable agreement of present results with the results of other authors yields sufficient confidence in the present numerical procedure and results.

For the case of the water droplets evaporation in the carrier gas, the following important conclusions are pointed out:

– As the carrier gas passes through the heated zone and its temperature is increased, its velocity vector gains an upward component due to the effect of buoyancy. Accordingly, hotter carrier gas exhibits motion in the upward direction associated with its motion in the axial direction.

– The lowest temperature gradient is produced in the lower wall region of heated furnace, and

consequently, the slower evaporation rate of the water droplets can be expected.

– Relative humidity of the carrier gas has no significant affect on the evaporation process.

References

1. Pokropivny, V. V. and Skorokhod, V. V. Classification of nanostructures by dimensionality and concept of surface forms engineering in nanomaterial science. 2007, Material Science Engineering, pp. 990-993.

2. Vert, M., et al., et al. Terminology for biorelated polymers and application (IUPAC Recommendations 2012). 2, 2012, Pure Appl. Chem., Vol. 84, pp. 377-410.

3. Okuyama, K. Preparation of micro-controlled particles using aerosol process. Journal of Aerosol Science, Volume 22, Supplement 1 (1991), 7-10.

4. Ogi, T., Hidayat, D., Iskandar, F., Purwanto, A., Okuyama, K. Direct synthesis of highly crystalline transparent conducting oxide nanoparticles by low pressure spray pyrolysis. Advanced Powder Technology, Volume 20, Issue 2 (2009), 203-209.

5. VDI Heat Atlas (Second Edition. Springer Verlag, Berlin (2010).

6. Morsi, S. A., alexander, A. J. An investigation of particle trajectories in two-phase flow systems. Journal of Fluid Mechanics, Volume 55, Issue 2 (1972), 193-208.

7. Ranz, W.E., Marshall, W.R. Evaporation from Drops, Part I. Chemical Engineering Progress, Volume 48 (1952), 141–146.

8. Miller, S., Harstad, K., Bella, J. Evaluation of Equilibrium and Non-Equilibrium Evaporation Models for Many Gas-Liquid Flow Simulations. International Journal of Multiphase Flow, Volume 24 (1998), 1025-1055.

9. Sazhin, S. S. Advanced Models of Fuel Droplet Heating and Evaporation. Progress in Energy and Combustion Science, Volume 32, Issue 2 (2006), 162-214.

10. Alroe, J. Modelling the Evaporation of a Liquid Droplet, http://vrs.amsi.org.au/wp-content/uploads/sites/6/2014/09ALROE_Joel._Research_Paper_revised.pdf .